Resource

Cell Reports

A Comprehensive Analysis of the Dynamic Response to Aphidicolin-Mediated Replication Stress Uncovers Targets for ATM and ATMIN

Graphical Abstract

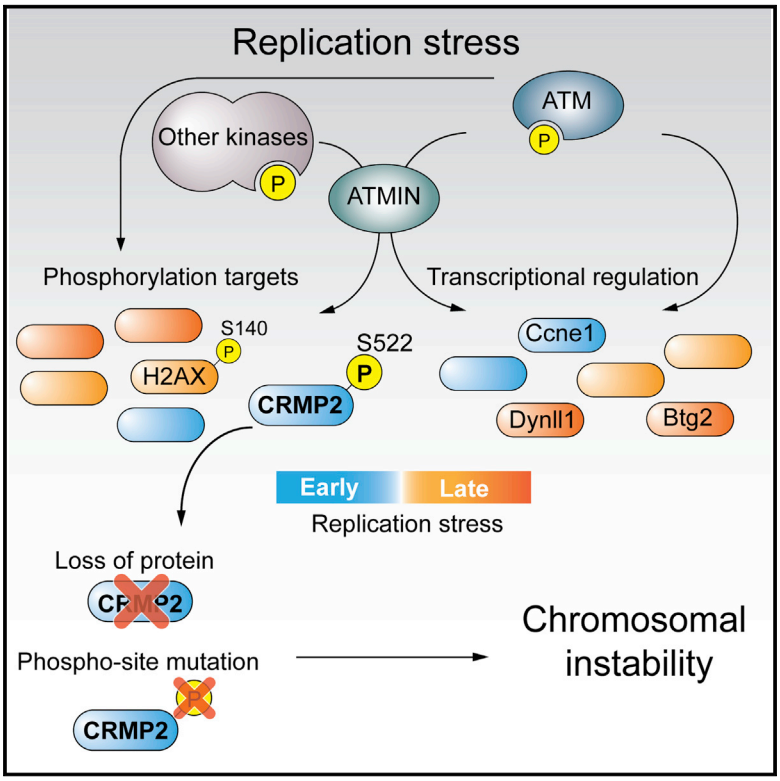

Highlights

- Replication stress triggers widespread changes in phosphorylation and expression
- ATM-ATMIN regulate phosphorylation events and expression upon replication stress
- ATMIN modulates the phosphorylation of H2AX and CRMP2 following replication stress
- Replication-stress-induced phosphorylation of CRMP2 regulates genome stability

Authors

Abdelghani Mazouzi, Alexey Stukalov, André C. Müller, ..., Jacques Colinge, Keiryn L. Bennett, Joanna I. Loizou

Correspondence

jloizou@cemm.oeaw.ac.at

In Brief

The global cellular response to replication stress is poorly understood. To elucidate the contribution of ATM-ATMIN signaling to the replication stress response, Mazouzi et al. combine phosphoproteomics and transcriptomics. They identify known and novel events, including the phosphorylation of CRMP2, a protein implicated in Alzheimer's disease but not in the DNA damage response.

Accession Numbers

GSE72275

Mazouzi et al., 2016, Cell Reports *15*, 1–16
April 26, 2016
http://dx.doi.org/10.1016/j.celrep.2016.03.077

CellPress

Please cite this article in press as: Mazouzi et al., A Comprehensive Analysis of the Dynamic Response to Aphidicolin-Mediated Replication Stress Uncovers Targets for ATM and ATMIN, Cell Reports (2016), http://dx.doi.org/10.1016/j.celrep.2016.03.077

Cell Reports
Resource

A Comprehensive Analysis of the Dynamic Response to Aphidicolin-Mediated Replication Stress Uncovers Targets for ATM and ATMIN

Abdelghani Mazouzi,[1] Alexey Stukalov,[1,2] André C. Müller,[1] Doris Chen,[1] Marc Wiedner,[1] Jana Prochazkova,[1] Shih-Chieh Chiang,[3] Michael Schuster,[1] Florian P. Breitwieser,[1,4] Andreas Pichlmair,[2] Sherif F. El-Khamisy,[3] Christoph Bock,[1] Robert Kralovics,[1] Jacques Colinge,[1,5] Keiryn L. Bennett,[1] and Joanna I. Loizou[1,*]

[1]CeMM Research Center for Molecular Medicine of the Austrian Academy of Sciences, Lazarettgasse 14, AKH BT 25.3, 1090 Vienna, Austria
[2]Max Planck Institute of Biochemistry, Am Klopferspitz 18, 82152 Martinsried, Germany
[3]Krebs Institute, Department of Molecular Biology and Biotechnology, University of Sheffield, Sheffield S10 2TN, UK
[4]Present address: McKusick-Nathans Institute of Genetic Medicine, Johns Hopkins University School of Medicine, Monument Street, Baltimore, MD 21205, USA
[5]Present address: Institut de Recherche en Cancérologie de Montpellier, Campus Val d'Aurelle, 34298 Montpellier Cedex 5, France
*Correspondence: jloizou@cemm.oeaw.ac.at
http://dx.doi.org/10.1016/j.celrep.2016.03.077

SUMMARY

The cellular response to replication stress requires the DNA-damage-responsive kinase ATM and its cofactor ATMIN; however, the roles of this signaling pathway following replication stress are unclear. To identify the functions of ATM and ATMIN in response to replication stress, we utilized both transcriptomics and quantitative mass-spectrometry-based phosphoproteomics. We found that replication stress induced by aphidicolin triggered widespread changes in both gene expression and protein phosphorylation patterns. These changes gave rise to distinct early and late replication stress responses. Furthermore, our analysis revealed previously unknown targets of ATM and ATMIN downstream of replication stress. We demonstrate ATMIN-dependent phosphorylation of H2AX and of CRMP2, a protein previously implicated in Alzheimer's disease but not in the DNA damage response. Overall, our dataset provides a comprehensive resource for discovering the cellular responses to replication stress and, potentially, associated pathologies.

INTRODUCTION

During DNA replication, genome integrity is challenged by factors that impede replication fork progression, hence resulting in replication stress (Mazouzi et al., 2014; Zeman and Cimprich, 2014). In turn, this can lead to replication fork collapse and consequently to the formation of DNA double-strand breaks (DSBs) (Fernandez-Capetillo and Nussenzweig, 2013; Toledo et al., 2013). Replication stress can be induced stochastically during cell-cycle progression or pathologically by the disregulation of oncogene expression, thus promoting oncogene induced transformation (Bartek et al., 2012; Halazonetis et al., 2008). Replication fork instability can also be triggered by exogenous agents such as aphidicolin (APH), which inhibits the replicative DNA polymerases (Glover et al., 1984) and leads to instability of particular genomic regions known as common fragile sites (CFSs). Such regions are particularly difficult to replicate and are susceptible to replication-stress-induced DSBs (Durkin and Glover, 2007). As such, these regions are hotspots for genomic aberrations (Wang et al., 1997).

To counteract DNA damage during DNA replication, cells have evolved a network of DNA damage surveillance pathways that maintain genome integrity. The DNA damage response is orchestrated by the PIKK kinases (phosphatidylinositol-3-kinase related kinases) Ataxia Telangiectasia Mutated protein (ATM); Ataxia Telangiectasia and Rad3 related protein (ATR); and DNA-dependent protein kinase, catalytic subunit (DNA-PKcs) that target a plethora of substrates for phosphorylation at serine or threonine residues followed by glutamine (the "SQ/TQ" motif) (Matsuoka et al., 2007). ATM and DNA-PKcs have most widely been studied in response to DNA DSBs, yet ATM has been reported to respond to diverse stimuli (Derheimer and Kastan, 2010; Kaidi and Jackson, 2013; Lavin and Kozlov, 2007). ATR is activated by its physical recruitment to single-stranded DNA (ssDNA), which can occur at persistent DSBs, but is found more extensively at stalled replication forks (López-Contreras and Fernandez-Capetillo, 2010). ATR and its downstream effectors can then delay cell-cycle progression and also stabilize stalled forks (Friedel et al., 2009). In addition to ATR, ATM is also required during the cellular response to replication stress (Harrigan et al., 2011; Lukas et al., 2011; Petermann and Helleday, 2010; Ward et al., 2005), yet its role has been largely underappreciated.

ATM is activated by two major cofactors—NBS1, which is part of the MRN complex (for MRE11-RAD50-NBS1), and ATMIN (ATM interactor; also known as ASCIZ for ATM substrate Chk2-interacting Zn^{2+}-finger protein)—in a stimulus-dependent manner (Kanu and Behrens, 2008). ATM is also activated after oxidative damage in a cofactor-independent manner (Guo et al., 2010). In response to DNA DSBs, the MRN complex leads

Please cite this article in press as: Mazouzi et al., A Comprehensive Analysis of the Dynamic Response to Aphidicolin-Mediated Replication Stress Uncovers Targets for ATM and ATMIN, Cell Reports (2016), http://dx.doi.org/10.1016/j.celrep.2016.03.077

to ATM activation (Difilippantonio et al., 2005; Falck et al., 2005; Lee and Paull, 2007; Uziel et al., 2003), while ATMIN is required for ATM activation upon replication stress (Kanu and Behrens, 2007; Kanu et al., 2015; Loizou et al., 2011; Schmidt et al., 2014).

Following replication stress, ATM has been shown to be required for recruiting DNA repair proteins, including 53BP1, to nuclear bodies at loci that are particularly susceptible to erosion, hence protecting these regions from degradation (Harrigan et al., 2011; Lukas et al., 2011). Furthermore, this event has been shown to occur in an ATMIN-dependent manner (Kanu et al., 2015; Schmidt et al., 2014). Within such genomic regions, OPT (for OCT-1, PTF, transcription) domains form in an ATM-dependent manner that represent regions of low transcriptional activity (Harrigan et al., 2011). Since these regions lack the phosphorylated, elongating forms of RNA polymerase II (Pol II), they denote regions of DNA damage that lead to transcription inhibition, which assists in the maintenance of genomic integrity (Harrigan et al., 2011).

Considering that both ATM and ATMIN are required for regulating the cellular response to replication stress, and yet their contribution to this fundamental cellular process is understudied, we devised an experimental system that would allow us to gain a comprehensive view of the events induced by replication stress. Furthermore, our system allowed us to delineate the contribution of ATM and ATMIN to this response in a global, unbiased, and time-resolved approach. We combined transcriptomics and quantitative mass spectrometry (MS)-based phosphoproteomics, in cells exposed to APH-induced replication stress, in a time-resolved manner. To map events dependent on the ATM signaling pathway, we utilized cells that have been genetically engineered to lack either ATM or ATMIN. Our study reveals that APH-induced replication stress leads to altered gene expression and that ATM and ATMIN contribute significantly to this effect. In parallel, we map widespread phosphorylation events on multiple proteins, in a time-dependent manner. Although some of the identified proteins and phosphorylation sites have already been implicated in the DNA damage response, a significant number has not. To validate our comprehensive data resource, we show that the phosphorylation of H2AX at serine 140 (also referred to as serine 139 in the mature protein; known as γH2AX in the phosphorylated form) occurs in an ATMIN-dependent manner upon exposure to replication stress. Furthermore, we identify CRMP2 as a replication-stress-induced phosphoprotein that requires ATMIN for its phosphorylation at S522. Phosphorylation at this site on CRMP2 is required for cell survival in response to replication stress. In summary, we have established the comprehensive and timed orchestration of gene expression and protein phosphorylation in known and novel sites (as well as proteins) that are involved in the cellular response to replication stress, induced by APH.

RESULTS

Charting the Global Cellular Response to Replication Stress

The cellular response to replication stress involves altering the expression of genes and the posttranslational modifications of proteins, including phosphorylation. To globally chart the cellular response to APH-induced replication stress over time, we took the following two approaches: using global phosphoproteomics, we quantified the changes in protein phosphorylation events by mass spectrometry, and using RNA sequencing (RNA-seq) we quantified the changes in the transcriptome. Furthermore, to delineate the contribution of the ATM-ATMIN signaling pathway, we performed these analyses in cells lacking either of these two proteins.

To determine the kinetics of DNA strand breaks induced by APH, we used the alkaline comet assay, which measures both DNA single- and double-strand breaks, and the neutral comet assay, which quantifies specifically DNA double-strand breaks. Mouse embryonic fibroblasts (MEFs) were treated with APH (1 μM) over a period of 24 hr. In response to APH treatment, DNA damage accumulated gradually over time (Figures 1A and 1B). This correlated with the increased localization of γH2AX and 53BP1 (two DNA damage markers) to damage sites (Figures 1C, S1A, and S1B). In its phosphorylated form, H2AX is crucial for the recruitment of DNA damage repair proteins in response to DSBs. Furthermore, H2AX has been previously shown to be phosphorylated in response to replication stress (Flach et al., 2014; Burhans and Weinberger, 2007). In addition, we noted that the early cellular stress response to APH (4 hr) did not affect cell-cycle progression, whereas prolonged stress for 24 hr caused a block in cell-cycle progression at S phase (Figures 1D and S1C).

Protein phosphorylation mediated by the ATM and ATR kinases is known to be important in signaling DNA replication stress. We measured ATM activation by examining the phosphorylation of known downstream targets, including KAP1 at S824 (mouse ortholog S823) and SMC1 at S957, and the autophosphorylation of ATM itself at S1981 (mouse ortholog S1987). Similarly, to monitor ATR activation we assessed the phosphorylation of CHEK1 at S345. We also monitored H2AX phosphorylation at S140 (γH2AX), which can be mediated by both ATM and ATR. Phosphorylation of ATR substrates is apparent within the first hour after APH treatment, whereas the phosphorylation of ATM substrates appeared between 2 hr and 12 hr (Figure 1E).

To identify the cellular response to replication stress (and to define the roles of ATM and ATMIN within this response), we performed transcriptomics and quantitative global phosphoproteomics at 4 hr and 24 hr post APH treatment (using *Atm*- and *Atmin*-deficient MEFs; Figure S1D). This approach allowed for global evaluation of the early and late events of replication stress signaling (Figure 1F).

Mapping Replication-Stress-Induced Transcriptional Events Dependent on ATM or ATMIN

To chart the transcriptional changes in response to replication stress, we performed RNA-seq of *Atm*- or *Atmin*-deficient MEFs ($Atm^{-/-}$ and $Atmin^{\Delta/\Delta}$) and their corresponding controls ($Atm^{+/+}$ and $Atmin^{+/+}$) at 4 hr and 24 hr post APH treatment. We defined APH-responsive genes as those shared between the two wild-type (WT) cell lines, when comparing APH treated to DMSO treated cells (Figure S2A), which led to the identification of 266 genes and 1,346 genes with significantly altered

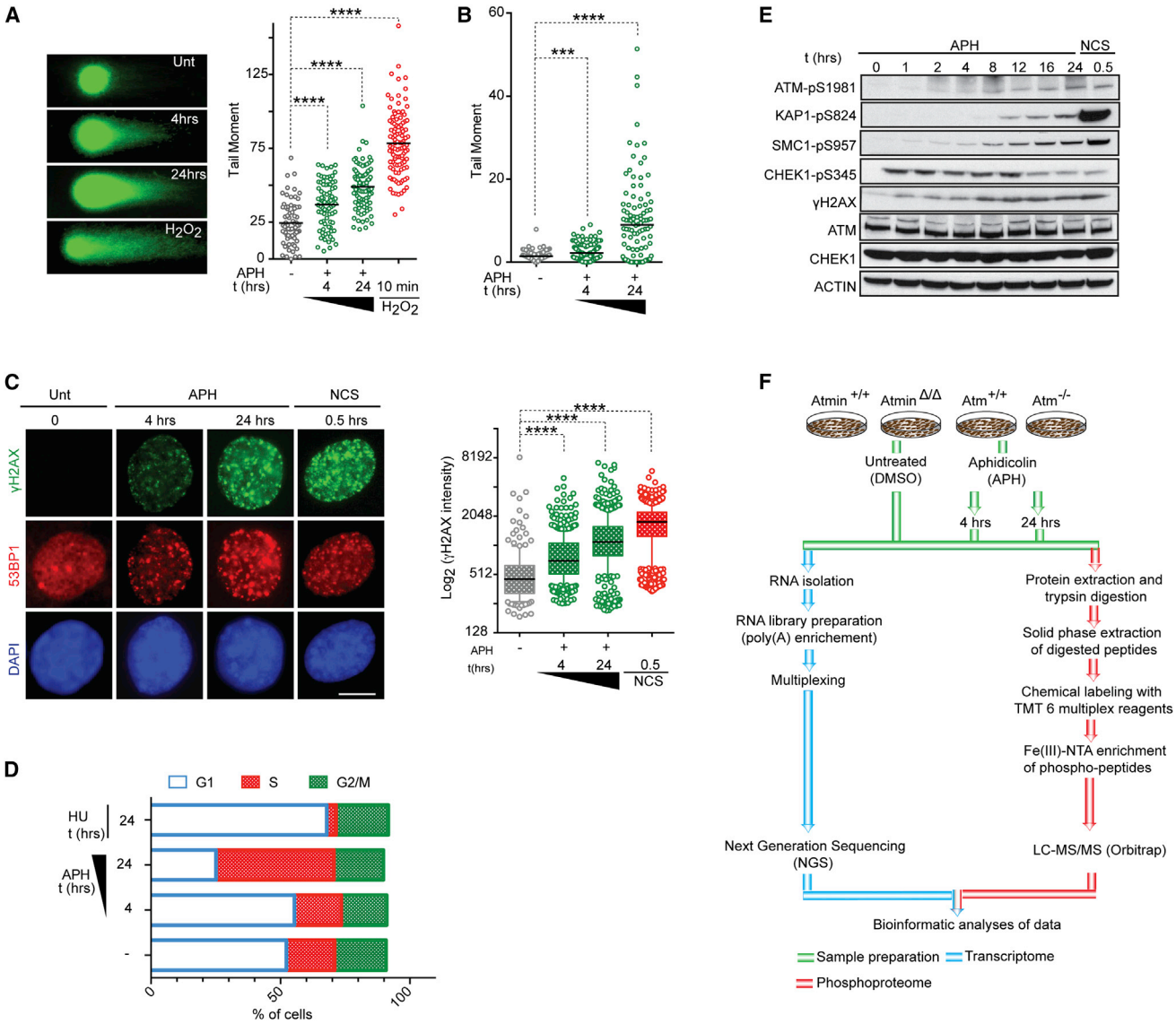

Figure 1. Mapping Early and Late APH-Induced Phosphorylation Events

(A) Left: DNA double- and single-strand breaks were detected, using the alkaline comet assay, in mouse embryonic fibroblasts (MEFs) treated with 1 μM aphidicolin (APH) for the indicated times or 100 μM H_2O_2 for 10 min. Right: box and whisker plot for the quantification of the tail moment of >100 cells.

(B) Box and whisker plot for the quantification of the tail moment using the neutral comet assay to measure specifically DNA double-strand breaks in MEFs treated with 1 μM APH for the indicated times.

(C) MEFs were treated with 1 μM APH or neocarzinostatin (NCS; a radiomimetic compound used as a positive control, at 50 ng/mL) for the indicated times and immunostained with anti-53BP1 and γH2AX antibodies, and nuclear DNA was counterstained with DAPI. Scale bar, 10 μm. Right: box and whisker plot for the quantification of γH2AX intensities displayed as a.u. of > 1,000 cells. ****$p < 0.0001$, ***$p < 0.001$ (p value was calculated by the Mann-Whitney U test).

(D) Analysis of cell-cycle progression of MEFs treated with 1 μM APH or 1 mM hydroxyurea (HU), for indicated times.

(E) Asynchronous MEFs were treated with APH (1 μM) or NCS for the indicated times. Whole-cell extracts were immunoblotted with the indicated antibodies.

(F) Schematic representation of the experimental setup used to identify roles for ATM and ATMIN in the cellular response to APH-induced replication stress. Transcriptomics and global phosphoproteomics were performed in *Atm*- and *Atmin*-deficient MEFs in the presence or absence of APH-induced replication stress at the indicated times.

expression using a multiple hypothesis adjusted p value of <0.01 (herein referred to as "adjusted p value") at 4 hr and 24 hr, respectively (Figures 2A and S2A). Eighty differential genes were shared between the two time points (Figure 2A). To determine the cellular processes predicted to be affected by replication stress, we performed gene ontology (GO) enrichment analysis on the genes significantly altered in expression upon exposure of WT MEFs to APH. Enriched biological processes

Please cite this article in press as: Mazouzi et al., A Comprehensive Analysis of the Dynamic Response to Aphidicolin-Mediated Replication Stress Uncovers Targets for ATM and ATMIN, Cell Reports (2016), http://dx.doi.org/10.1016/j.celrep.2016.03.077

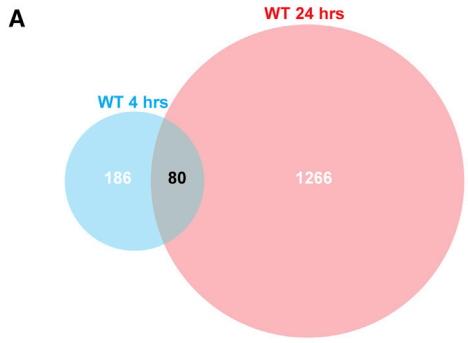

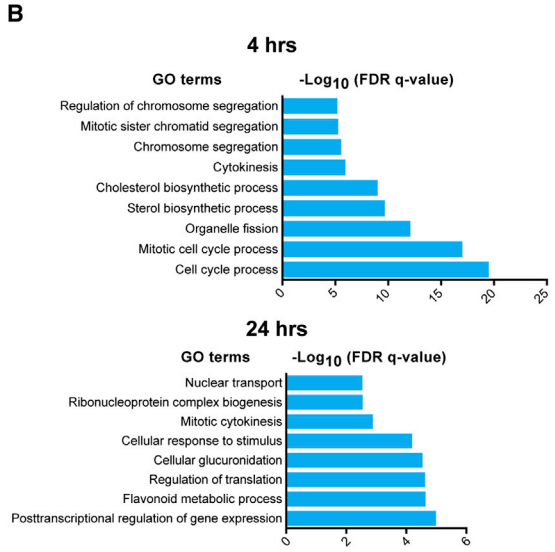

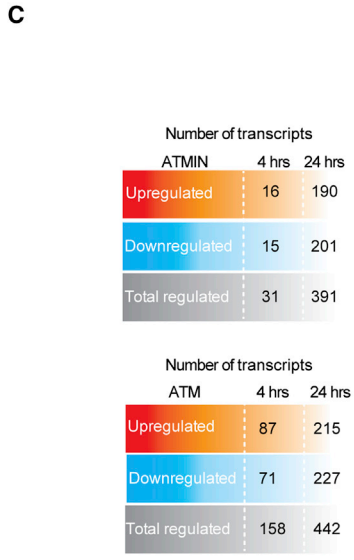

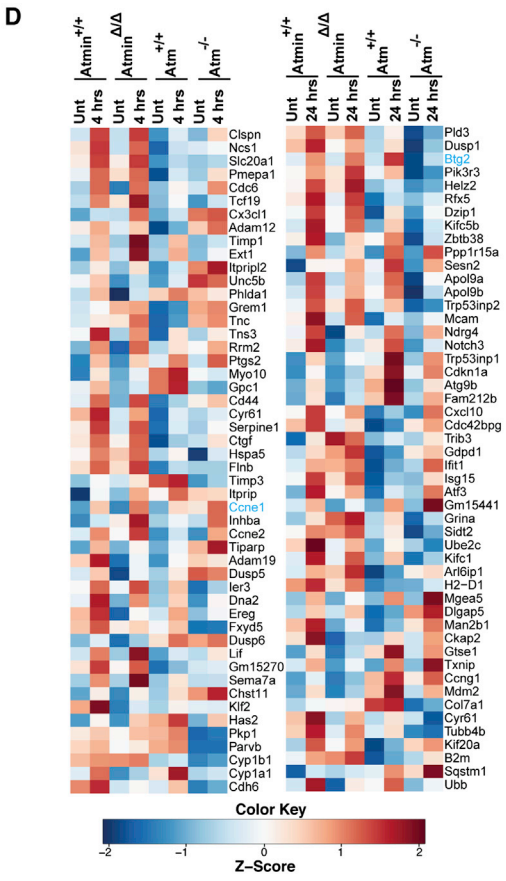

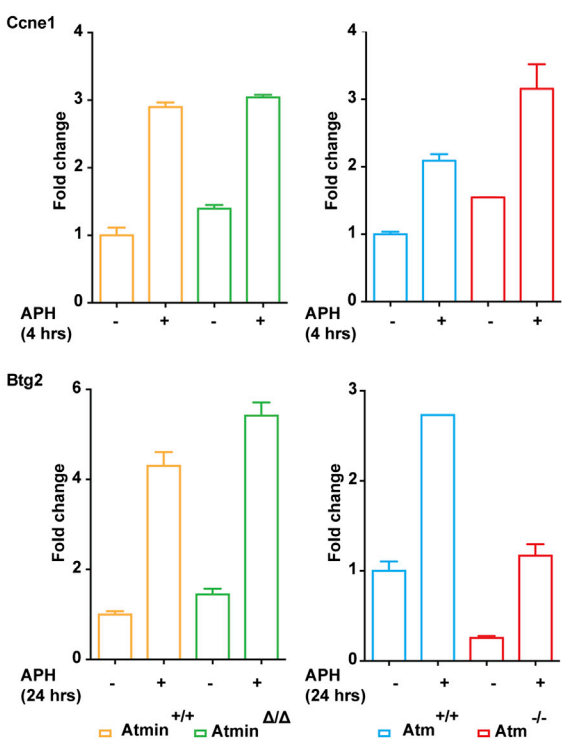

(legend on next page)

at 4 hr and 24 hr post APH treatment included those related to cell-cycle regulation and response to stimuli (Figures 2B and S2B).

Next, we identified APH responsive genes that require ATMIN or ATM as those genes that are APH responsive in WT cells but not in ATMIN- or ATM-deficient cells (Figure S2A). By applying an adjusted p value cutoff of <0.01, we found that ATM influenced the expression of around 59.4% and 32.8% of APH-responsive genes at 4 hr and 24 hr post treatment, respectively, compared to ATMIN, which modulated the expression of 11.7% at 4 hr and 29% at 24 hr post APH treatment genes (Figures 2C, S2A, and S2C; Table S1). These data highlight the importance of both ATM and ATMIN in regulating gene expression following replication stress induced by APH, but also reveal their requirement in regulating gene expression in the absence of exogenous stress (Figure S2D). The 50 most significantly downregulated genes in *Atmin*-deficient or *Atm*-deficient cells are displayed in Figure S2E. The effect of ATMIN or ATM loss on the expression of the 50 most significantly upregulated APH responsive genes in WT cells is shown in Figure 2D. Among these, the expression of several genes required for cell-cycle regulation was altered in an ATMIN- and/or ATM-dependent manner, including Cyclin E1 (*Ccne1*) and B Cell Translocation Gene 2 (*Btg2*) (Figure 2D). BTG2 plays an important role in the regulation of the cell division cycle via downregulation of *Ccne1* biosynthesis, along with CDK4 activity (Corrente et al., 2002). qRT-PCR was used to independently confirm these data (Figure 2E). In summary, this dataset has allowed for the identification of APH responsive genes and moreover has revealed the extent to which ATM and ATMIN are required to alter the regulation of these genes.

Time-Resolved Phosphorylation Dynamics Mediated by ATM and ATMIN in Response to Replication Stress

Next, we investigated the impact of replication stress on protein phosphorylation and the requirement of ATM and ATMIN in this process. By analyzing WT cells as well as *Atm*- and *Atmin*-deficient cells in the presence or absence of APH (4 hr and 24 hr APH exposure), we identified a total of 13,801 unique phosphorylation sites within 4,094 proteins, with a false discovery rate (FDR) of <0.1% for peptide and <1% for proteins (Figure 3A). The distribution of the individual phosphorylated residues (serine [S] = 80.6%, threonine [T] = 16.7%, tyrosine [Y] = 2.7%) and the number of phosphoryl groups per peptide were comparable to published data (Bensimon et al., 2010; Bodenmiller et al., 2007; Olsen et al., 2006) (Figures 3A and S3A). Of the identified phosphorylation sites, 27.3% have not been reported previously in the PhosphoSitePlus database (Figure 3B).

We defined significant time-resolved APH-induced alterations in phosphopeptides in WT MEFs using both an adjusted p value cutoff of 0.05 (herein referred to as the "confident" sites; blue dashed line) as well as a more stringent unadjusted p value cutoff of 0.001 (herein referred to as the "less stringent" sites; black dashed line) (Figures 3C, 3D, and S3B). Our motivation in selecting these two cutoffs was to acquire a broader perspective of the phosphorylation landscape. We illustrate the phosphorylation of proteins known to be required for DNA replication, the DNA damage response, and cell-cycle progression as green dots in Figures 3C and 3D. For example, following early replication stress, we observed phosphorylation of H2AX (at S137 and S140), CDK2/3 (at T14 and Y15), TP53 (S307; p53), MCM3 (T719), and RIF1 (S1565). Following late replication stress, we identified additional phosphorylation sites on H2AX (S121, S122, S137, and S140). We also identified phosphorylation sites on BRCA1 (S686, S706, S717), MCM6 (S704 and S762), MDC1 (S157, S176, and S943), SMC3 (S1065 and S1067), RFC1 (S281), TP53 (S307 and S309), and TRIM28 (S473; KAP1), among many others (Figures 3C and 3D; Tables S2 and S3). Of note, phosphorylation of MDC1 at S943 and of RFC1 at S281 had not previously been identified. To identify which pathways are represented by changes in phosphorylation events following APH exposure, we used GO enrichment analyses. This revealed the pathways of nucleic acid metabolism and chromatin assembly and/or disassembly to be among the most significantly represented at 4 hr post APH treatment (Figure 3E). At 24 hr post APH, the pathways of cell cycle, DNA repair, DNA damage response, and nucleosome assembly were most significantly enriched (Figure 3E).

To gain insights into the protein sequences that were preferentially phosphorylated upon APH treatment, we generated a motif representation of the overrepresented phosphosites (Figures 3F and S3C). The ATM superfamily of kinases is known to target SQ/TQ substrate motifs for phosphorylation. As expected, we identified the SQ motif in the group of sites that increased in phosphorylation, comprising ~50% of the detected replication-stress-responsive phosphorylation sites at 4 hr and a relatively small fraction (~10%) at 24 hr. Other overrepresented motifs were SP, SD, TP, and TE (Figures 3F and S3C), which is in line with phosphorylation events reported in response to the radiomimetic drug neocarzinostatin (NCS), which generates DNA double-strand breaks, as well as other lesions (Bensimon et al., 2010).

Figure 2. Dynamic Analyses of Transcriptional Responses to APH-Induced Replication Stress

(A) Venn diagram illustrating the overlap of genes that are differentially expressed (adjusted p value < 0.01) in both wild-type MEF cell lines treated with APH for 4 hr or 24 hr compared to untreated cells.

(B) Gene ontology (GO) enrichment analysis of the significantly differentially expressed genes in wild-type MEFs upon APH treatment (1 μM APH compared to DMSO), at the indicated times. The x axis represents $-\log_{10}$ values of the multiple-test corrected p values.

(C) Numbers of APH-responsive transcripts that are ATM or ATMIN dependent at 4 hr or 24 hr post treatment (adjusted p value < 0.01). See Figure S2A for details.

(D) Heatmaps illustrating the 50 most significantly upregulated APH responsive genes in both wild-type MEF cell lines treated for 4 hr or 24 hr compared to DMSO. The effects of ATMIN and ATM deficiencies on the expression of these genes are displayed as well. Genes marked in blue are validated experimentally in (E). *Z* score normalized values are shown.

(E) mRNA expression analysis of indicated genes by qRT-PCR. Expression of mEF1α was used as a reference. Error bars indicate SEM (n = 2). GO, gene ontology; Unt, untreated.

Please cite this article in press as: Mazouzi et al., A Comprehensive Analysis of the Dynamic Response to Aphidicolin-Mediated Replication Stress Uncovers Targets for ATM and ATMIN, Cell Reports (2016), http://dx.doi.org/10.1016/j.celrep.2016.03.077

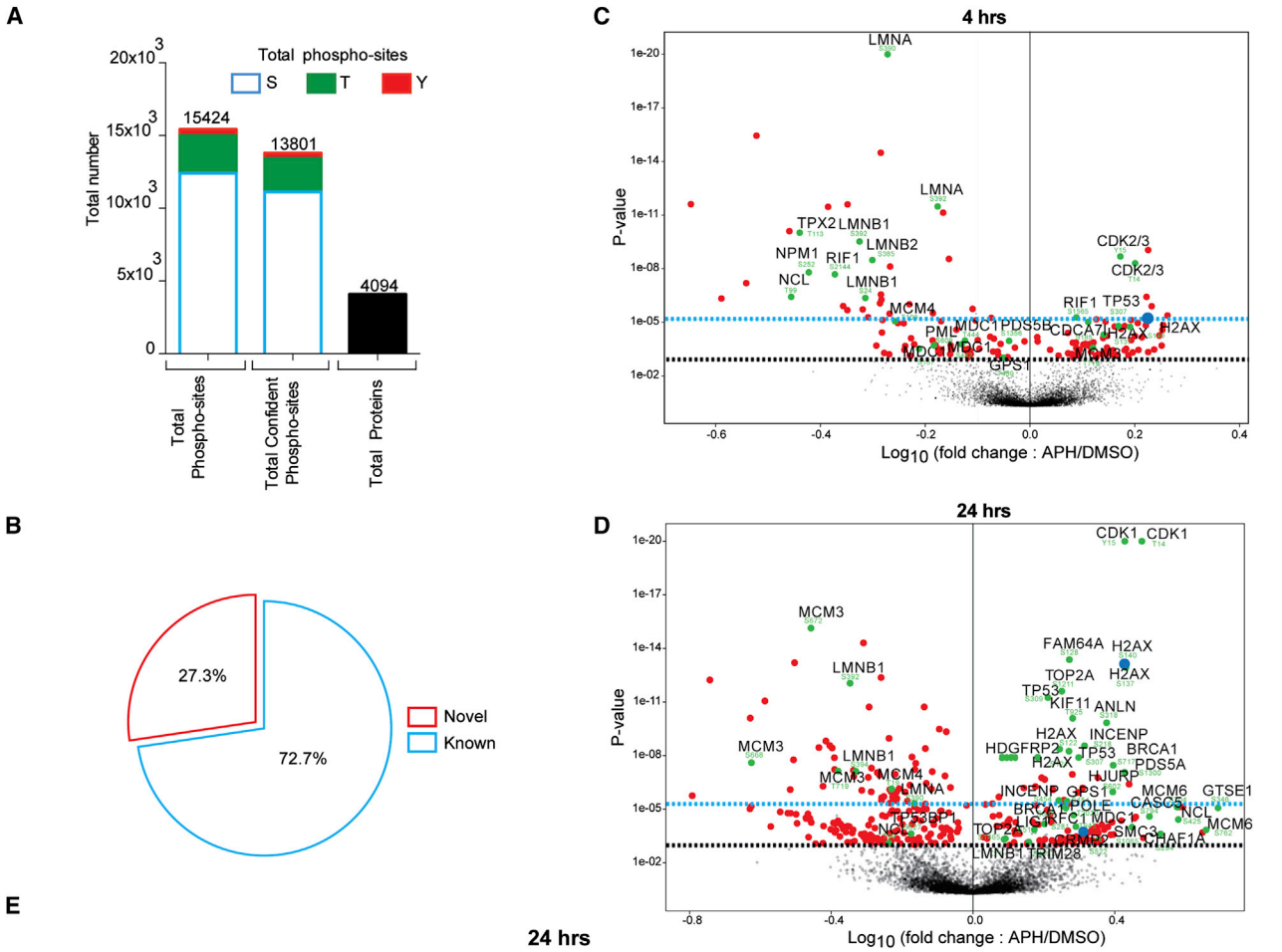

(legend on next page)

Using the same analytical approach utilized previously for gene expression (Figure S2A), we identified 73.8% of phosphorylation sites to be modulated by ATM following early replication stress (4 hr [Figures 3G and S3D], by applying a p value cutoff of 0.001; data correlating the biological replicates at early and late time points are shown in Figure S3E). These data highlight an important role for ATM in the early response to replication stress induced by APH. Around 52.6% of the APH-induced phosphorylation events were found to be regulated by ATM at the late time point of 24 hr. At early replication stress (4 hr) ATMIN modulated 46.2% of the APH-responsive phosphorylation sites compared to 66.7% for 24 hr post treatment. Approximately 30% of the APH-dependent phosphorylation sites that are ATM dependent are also ATMIN dependent, hence demonstrating the importance of ATMIN as an ATM cofactor (Figure S3D). Yet, the phosphorylation sites that are not shared between ATMIN and ATM raise the possibility that ATMIN potentially regulates these phosphorylation events on multiple substrates independently of ATM (Figures 3G and S3D).

Next, we systematically investigate the dynamic relationship between putative kinase-substrate and phosphatase-substrate networks that may correspond to the phosphosites regulated by replication stress using the NetworKIN software (Horn et al., 2014). In addition to ATM and PRKDC (DNA-PKcs) (Figure S4, blue squares), multiple other kinases were predicted to respond to replication stress based on the observed phosphosite changes (gray squares) including CDKs and ABL1, among many others. These results suggest that replication-stress-induced phosphorylation mediated via the use of APH is considerably wider than PIKK-mediated phosphorylation events.

ATMIN Mediates the Phosphorylation of Multiple Substrates in a Stress- Dependent Manner

An additional analytical approach was taken to display ATM- or ATMIN-dependent phosphorylation substrates. First, ATMIN- or ATM-deficient cell lines were compared to their corresponding WT cells (in the presence or absence of APH) (Figure S3F). Next, the significant ATM- or ATMIN-dependent phosphorylation sites were selected if they were APH responsive in WT cells and unchanged in unperturbed cells (Figures 4A and S5, blue and red dots). This led to the identification of several ATMIN-dependent phosphorylation sites on proteins known to be involved in the DNA damage response, as noted by the altered phosphorylation of several DNA replication and repair factors (Figure 4A, green hollow circles). At 4 hr post APH treatment the following ATMIN-dependent phosphoproteins, among others, were diminished in phosphorylation: RIF1 (at S2144), PML (at S609), and MCM4 (at T109) (Table S3). At 24 hr post APH, the following ATMIN-dependent phosphoproteins were reduced in phosphorylation: POLE (at T2020), PML (at S490), and MCM6 (at S704) (Table S3). We identified H2AX (also known as H2AFX) to be phosphorylated upon APH treatment in an ATMIN-dependent manner (at S140) at 4 hr post APH treatment and at two phosphorylation sites (S122 and S140) at 24 hr post APH exposure.

We constructed a putative ATMIN-dependent kinase/phosphatase-substrate network using NetworKIN for all the significantly induced phosphorylation sites by comparing WT cells to ATMIN-deficient cells following APH treatment, over time (Figure 4B; ATMIN-dependent substrates are illustrated as red octagons with black borders). The resulting network revealed substantial involvement of multiple kinases dependent on ATMIN for the cellular response to replication stress, including CDK5 and GSK3B (Figure 4B).

ATMIN is an essential Zn^{+2} finger protein that functions as a transcription factor during development, where it regulates expression of Dynll1 (Figure S2E) (Jurado et al., 2012). To exclude the possibility that ATMIN regulates the identified phosphoproteins via transcription, similarly we investigated the expression levels of all the significantly induced phosphproteins by comparing WT cells to ATMIN-deficient cells (4 hr and 24 hr post APH treatment). Given the good reproducibility of the biological replicates (Figure S6A), we were able to exclude ATMIN-dependent genes (Figure 4A) that displayed altered expression upon loss of ATMIN (Figure S6B), hence leading to the identification of ATMIN-dependent phosphorylation substrates that are independent of transcription (Figure 4C, bold).

H2AX Phosphorylation in Response to APH Requires ATMIN

We chose to validate the phosphorylation of H2AX at S140 (γH2AX) that we observed to be both affected by APH treatment and ATMIN dependent (Figures 3C, 3D, and 4A, dark blue dots; Figure 5A). Manual inspection of the respective MS spectrum

Figure 3. Identification of Proteome-wide Phosphorylation Changes Dependent on ATM and ATMIN, in Response to APH-Induced Replication Stress

(A) Total number of phosphorylation sites and proteins, which were confidently identified. The proportion of phosphorylated serine (S), threonine (T), and tyrosine (Y) residues is also indicated.

(B) Percentage of novel and known phosphorylation sites identified based on the PhosphoSitePlus database.

(C and D) Analysis of phosphorylation events occurring in wild-type MEFs treated with 1 μM APH for 4 hr (C) or 24 hr (D), compared to DMSO treated cells. Volcano plots display the decimal logarithm of the fold change plotted against the p value. Black dashed lines indicate the significance cutoff for the identification of "confident" sites, and blue dashed lines indicates the significance cutoff for the identification of "less stringent" sites (as defined in the manuscript). Green dots indicate phosphorylation sites on DNA damage response proteins. Red dots indicate phosphorylation sites on other proteins that have not previously been implicated in the DNA damage response. Blue dots indicate the phosphorylation of H2AX at S140 that is validated experimental in following sections.

(E) Gene ontology (GO) enrichment analysis of the significantly increased (red) or decreased (blue) phosphorylation events in wild-type MEFs upon APH treatment (1 μM APH compared to DMSO), at the indicated times. The x axis represents the $-\log_{10}$ of the p value.

(F) Ice-Logo plots indicating the frequency of five amino acids flanking each side of phosphorylated serine residues (0 position) that are significantly increased in phosphorylation in wild-type MEFs (APH compared to DMSO) at the indicated times.

(G) Number of ATMIN- and ATM-dependent phosphorylation sites induced upon APH treatment at 4 hr or 24 hr.

See Figure S3D for details.

Please cite this article in press as: Mazouzi et al., A Comprehensive Analysis of the Dynamic Response to Aphidicolin-Mediated Replication Stress Uncovers Targets for ATM and ATMIN, Cell Reports (2016), http://dx.doi.org/10.1016/j.celrep.2016.03.077

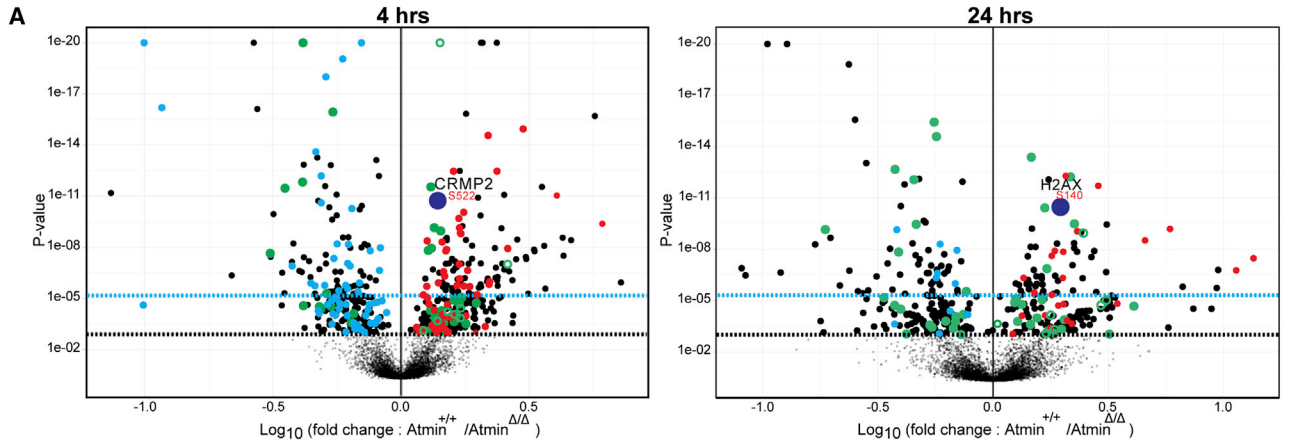

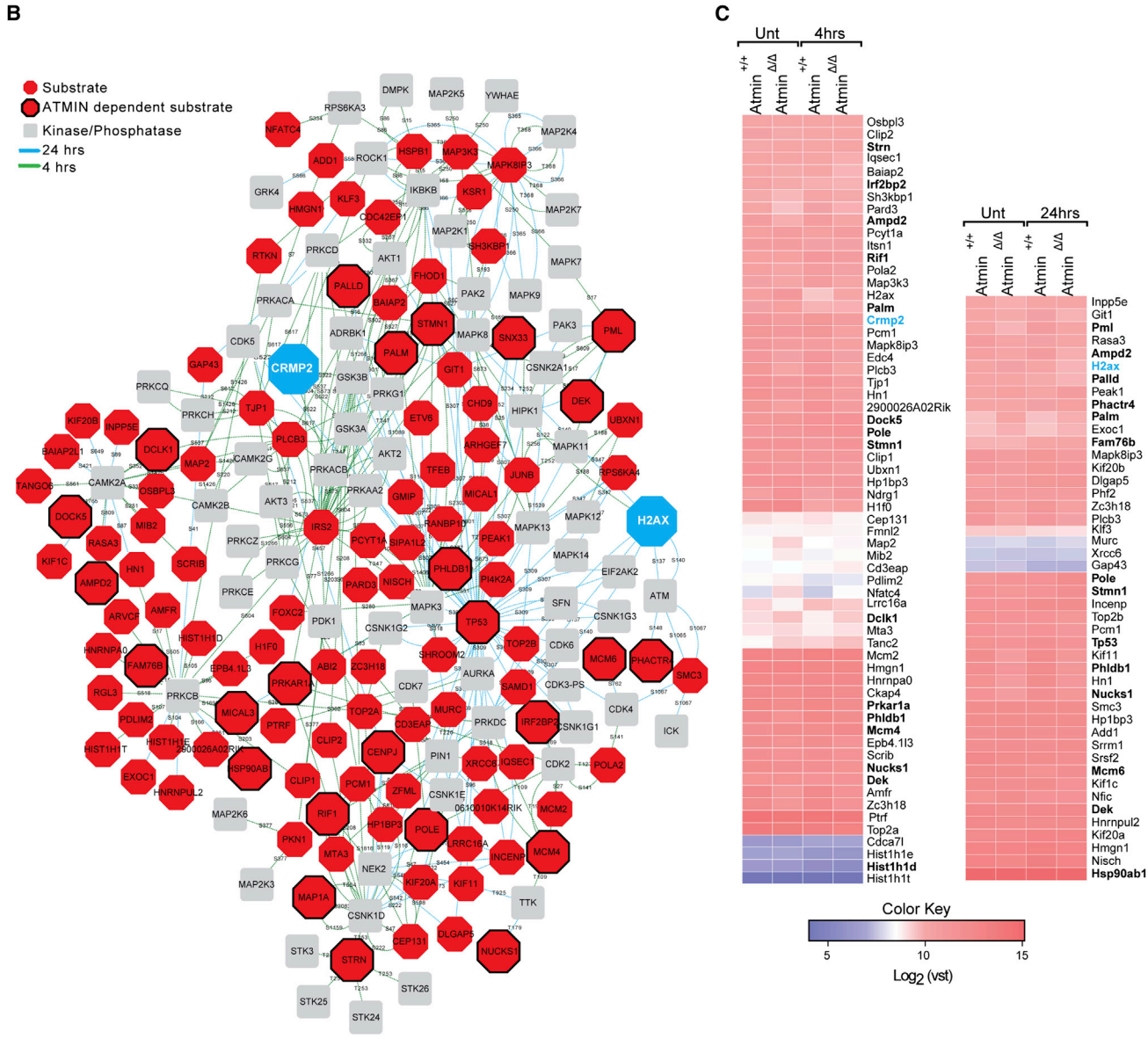

(legend on next page)

confirmed the correct identification and phosphosite assignment of S140 on H2AX (Figure 5B). Immunoblotting provided further support for a reduction in the APH-induced phosphorylation of H2AX in cells lacking ATMIN, at both early and late time points after treatment (Figure 5C). Moreover, immunofluorescence indicated that although γH2AX accumulated in control MEFs upon APH treatment, this was reduced in MEFs lacking ATMIN (Figures 5D and 5E). Taken together, these data confirm the results of the MS-based approach that identified ATMIN-dependent γH2AX accumulation.

Next, we investigated the effect of ATMIN on the clearance of γH2AX. We found that γH2AX decreased over a 6-hr repair period upon removal of APH from WT cells. In contrast, the phosphorylation of H2AX remained substantially low, but unchanged, in ATMIN-null cells 6 hr after APH removal (Figure 5F). Thus, ATMIN appears to promote the accumulation of γH2AX during the DNA damage response.

CRMP2 Is a Replication-Dependent Phosphoprotein Requiring ATMIN

Next, we chose to validate the ATMIN- and APH-dependent phosphorylation of the Collapsin response mediator protein-2 (CRMP2), a protein not previously implicated in the DNA damage response. CRMP2 (also known as DPYSL2) is a largely cytosolic multifunctional adaptor protein that has been shown to mediate the addition of tubulin dimers to the growing microtubule (Fukata et al., 2002). Additionally, CRMP2 has high sequence homology to the dihydropyrimidinase enzymes (DPYS) responsible for uracil and thymine catabolism; however, CRMP2 itself has no known enzymatic activity. CRMP2 has also been studied extensively in the context of the CNS and is associated with several neuropathological or psychiatric conditions including Alzheimer's disease (AD) and schizophrenia (Hensley et al., 2011). CRMP2 appears to be involved in many essential neurophysiological functions as well as in different cellular processes in other tissues including vesicle transport, migration, and mitosis (Hensley et al., 2011). Interestingly, nuclear CRMP-2 phosphorylated at T514 has been linked to poor prognosis in non-small-cell lung cancer (NSCLC) and was found to interact with the mitotic spindle in a phosphorylation-dependent manner in NSCLC cells (Oliemuller et al., 2013). Given these observations, we decided to investigate the role of CRMP2 phosphorylation induced by replication stress. First, we treated ATMIN-proficient and -deficient MEFs with APH for 4 hr or 24 hr. We noted a time-dependent increase in the phosphorylation of CRMP2 at S522 in WT cells, but not cells lacking ATMIN (Figure 6A), supporting the MS data (Figures 3D and 4A, dark blue dot). Importantly, the total protein levels of CRMP2 remained unchanged in response to replication stress and/or loss of ATMIN. We confirmed these findings by immunofluorescence, where we noted a time- and ATMIN-dependent increase in phosphorylation of CRMP2-S522 upon APH treatment of MEF cells (Figures 6B and 6C). The specificity of the phospho-S522 CRMP2 antibody is illustrated in Figure S7A.

To understand the cellular function of CRMP2 and the APH-induced phosphorylation of S522, we generated CRMP2-depleted cells using three independent short hairpin RNAs (shRNAs) (Figure 6D). Cell-cycle analysis of human A549 cells treated with APH for different durations showed that the distribution of G1, S, and G2/M populations in cells expressing CRMP2-specific shRNAs was comparable to control cells (Figure S7B). However, loss of CRMP2 impaired cell-cycle progression recovery following APH-induced stress. Surprisingly, upon release from APH-induced stress, cells depleted for CRMP2 showed a blockage in G1 and delayed progression through S phase (Figure S7C), suggesting that CRMP2 is involved in the resumption of normal cell-cycle kinetics following replication stress.

Efficient depletion of CRMP2 also triggered an increase in phosphorylation of TP53 at S15 upon APH treatment, indicative of increased apoptosis and/or cell-cycle arrest (Kruse and Gu, 2009; Shaw, 1996) (Figure 6D). To determine whether CRMP2-depleted cells display increased levels of DNA damage in response to APH, triggering increased S15-TP53, we evaluated H2AX phosphorylation. Depletion of CRMP2 led to diminished levels of γH2AX both by immunoblotting (Figure 6E) and immunofluorescence (Figures 6F, 6G, S7D, and S7E). Under these conditions phosphorylation of the ATM target, KAP1, was modestly effected (Figure 6E). Furthermore, the two shRNAs that gave the most pronounced knockdown of CRMP2 (shCRMP2-1 and shCRMP2-2) vastly reduced survival and proliferation as measured by a clonogenic assay (Figure S7F). A hallmark of H2AX-deficient cells is an accumulation of chromosomal

Figure 4. ATMIN Is an Important Regulator of APH-Induced Phosphorylation

(A) Analysis of APH-induced phosphorylation sites in wild-type (*Atmin*$^{+/+}$) cells compared to ATMIN-deficient cells (*Atmin*$^{\Delta/\Delta}$) in a time-dependent manner. Volcano plot shows the decimal logarithm of the fold change and the p value. Black dashed lines indicate the significance cutoff for the identification of "confident" sites, and blue dashed lines indicate the significance cutoff for the identification of "less stringent" sites, as previously defined. Green dots represent phosphorylation sites that occur on known DNA damage response proteins. ATMIN-dependent phosphorylation sites that are induced by APH are represented by red dots, and sites that are reduced upon APH treatment in an ATMIN-dependent manner are represented by blue dots. Green hollow circles represent ATMIN-dependent phosphorylation sites that occur in on known DNA damage response proteins. Black dots represent all remaining APH-induced phosphorylation sites obtained by comparing wild-type (*Atmin*$^{+/+}$) cells to ATMIN-deficient cells (*Atmin*$^{\Delta/\Delta}$). The two dark blue dots highlight two ATMIN- and APH-dependent substrates (CRMP2-S522 and H2AX-S140) validated experimentally in following sections.

(B) NetworKIN predictions of the kinase-substrate and phosphatase-substrate networks for APH-induced phosphorylation sites that are reduced in ATMIN-deficient cells (*Atmin*$^{\Delta/\Delta}$) compared to wild-type (*Atmin*$^{+/+}$) cells. Gray squares denote kinases or phosphatases and red octagons denote their substrates. Red octagons with black borders represent ATMIN-dependent substrates. The edges indicate phosphorylation events occurring at 4 hr (green edges) and 24 hr (blue edges) post APH. The edges are annotated with the corresponding phosphorylation sites. The blue octagons denote two ATMIN- and APH-dependent substrates (CRMP2-S522 and H2AX-S140) validated experimentally in the following sections.

(C) mRNA expression levels of phosphoproteins that are ATMIN dependent and are not differentially expressed are illustrated with bold gene names. Expression values were obtained from the mean of two biological replicates. Genes in blue are validated experimentally in the following sections. Vst, variance-stabilizing transformation.

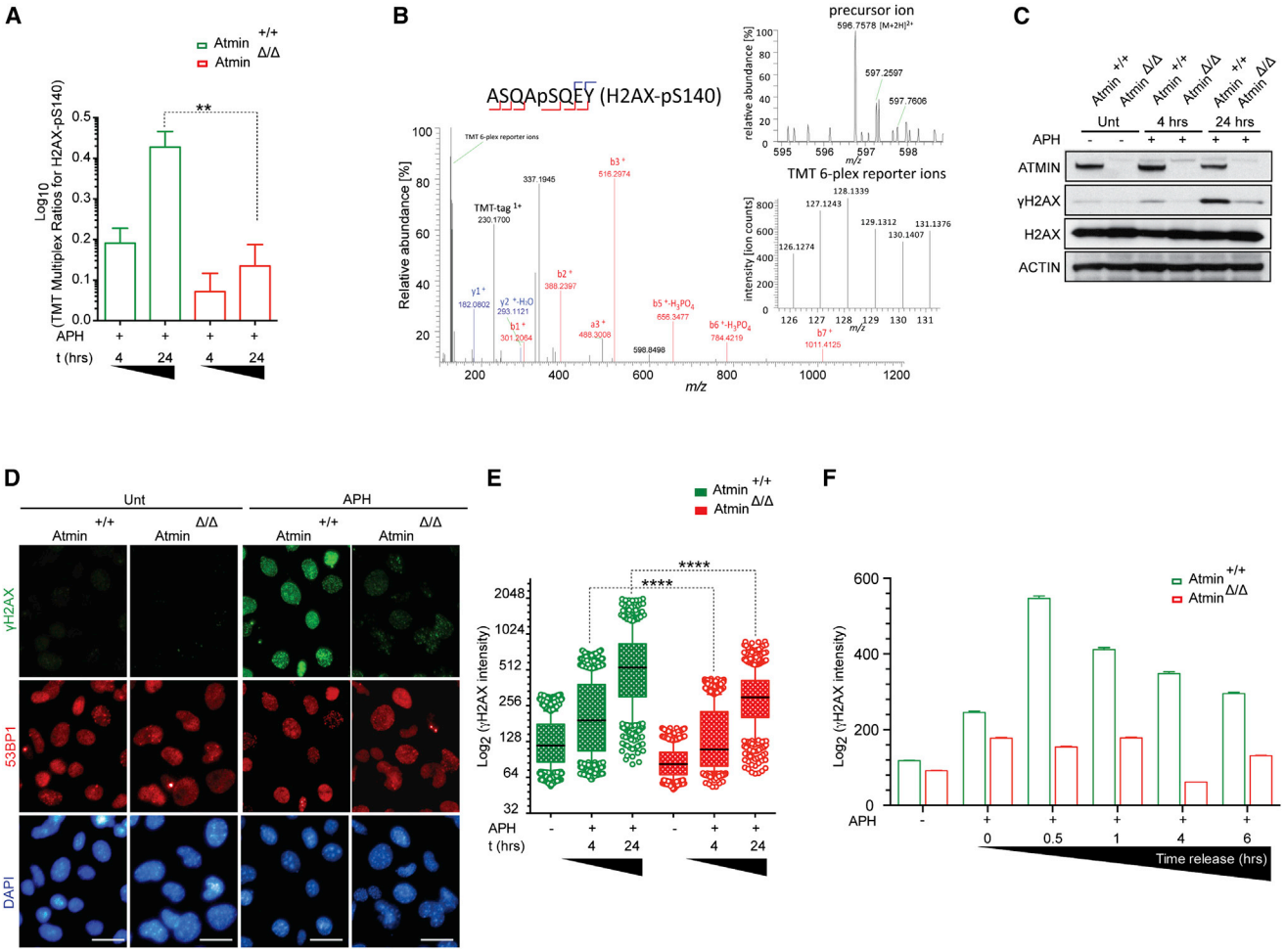

Figure 5. H2AX Requires ATMIN for Phosphorylation upon APH-Induced Replication Stress

(A) TMT Multiplex Ratios of H2AX phosphorylated at Ser-140 in ATMIN wild-type (*Atmin*$^{+/+}$) in comparison to ATMIN-deficient (*Atmin*$^{\Delta/\Delta}$) MEFs treated with APH. Data are normalized to *Atmin*$^{+/+}$ MEFs treated with DMSO at the indicated time points.

(B) TMT mass spectrometry spectra for H2AX (S140) phosphopeptide.

(C) *Atmin*$^{+/+}$ and *Atmin*$^{\Delta/\Delta}$ MEFs were treated with 1 μM APH for 4 hr or 24 hr and phosphorylation of H2AX at S-140 (known as γH2AX) was analyzed by immunoblotting.

(D) *Atmin*$^{+/+}$ and *Atmin*$^{\Delta/\Delta}$ MEFs were treated with 1 μM APH for 24 hr and immunostained with γH2AX and 53BP1 antibodies. Nuclear DNA was counterstained with DAPI. Scale bar, 10 μm.

(E) The quantification of γH2AX intensities per nucleus of *Atmin*$^{+/+}$ and *Atmin*$^{\Delta/\Delta}$ MEFs in the presence or absence of 1 μM APH (for the indicated times) of more than 1,000 cells. Black lines within each column represent median intensities. ****$p < 0.0001$ (p value was calculated by the Mann-Whitney U test).

(F) *Atmin*$^{+/+}$ and *Atmin*$^{\Delta/\Delta}$ MEFs were treated with 1 μM APH for 24 hr and then released into compound-free medium for the indicated time points. Cells were immunostained for γH2AX and displayed are γH2AX intensities per nucleus quantified for more than 1,000 cells. Error bars indicate SEM.

aberrations (Celeste et al., 2002). Indeed, CRMP2-depleted cells displayed increased micronuclei upon exposure to APH compared to control cells (Figure 6H). Taken together, these data indicate a requirement of CRMP2 to clear DNA damage upon exposure to replication stress, by preventing micronuclei formation. This could potentially be mediated via CRMP2-dependent phosphorylation of H2AX.

To investigate the role of phosphorylation of CRMP2 at S522, we reconstituted shCRMP2-3 cells (this shRNA does not affect proliferation, as opposed to shCRMP2-1 and -2) with either WT CRMP2 or CRMP2 carrying a serine to alanine mutation at position 522. We had observed that CRMP2 depletion increased the sensitivity of A549 cells to hydroxyurea (HU). HU is an alternative agent that induces replication stress by blocking the synthesis of deoxynucleotides, thus inhibiting DNA synthesis and inducing cell death more potently than APH (Figures 7A and 7B). We found that this sensitivity could be rescued by reconstitution with WT, but not with the S522A phospho mutant CRMP2 (Figures 7A–7C). Additionally, although reconstitution with the WT CRMP2 could rescue the increased sub-G1 population of apoptotic cells upon APH treatment, the S522A phospho mutant could not (Figure 7D). These data indicate that the ATMIN-mediated phosphorylation of CRMP2 is required to suppress apoptosis in response to replication stress.

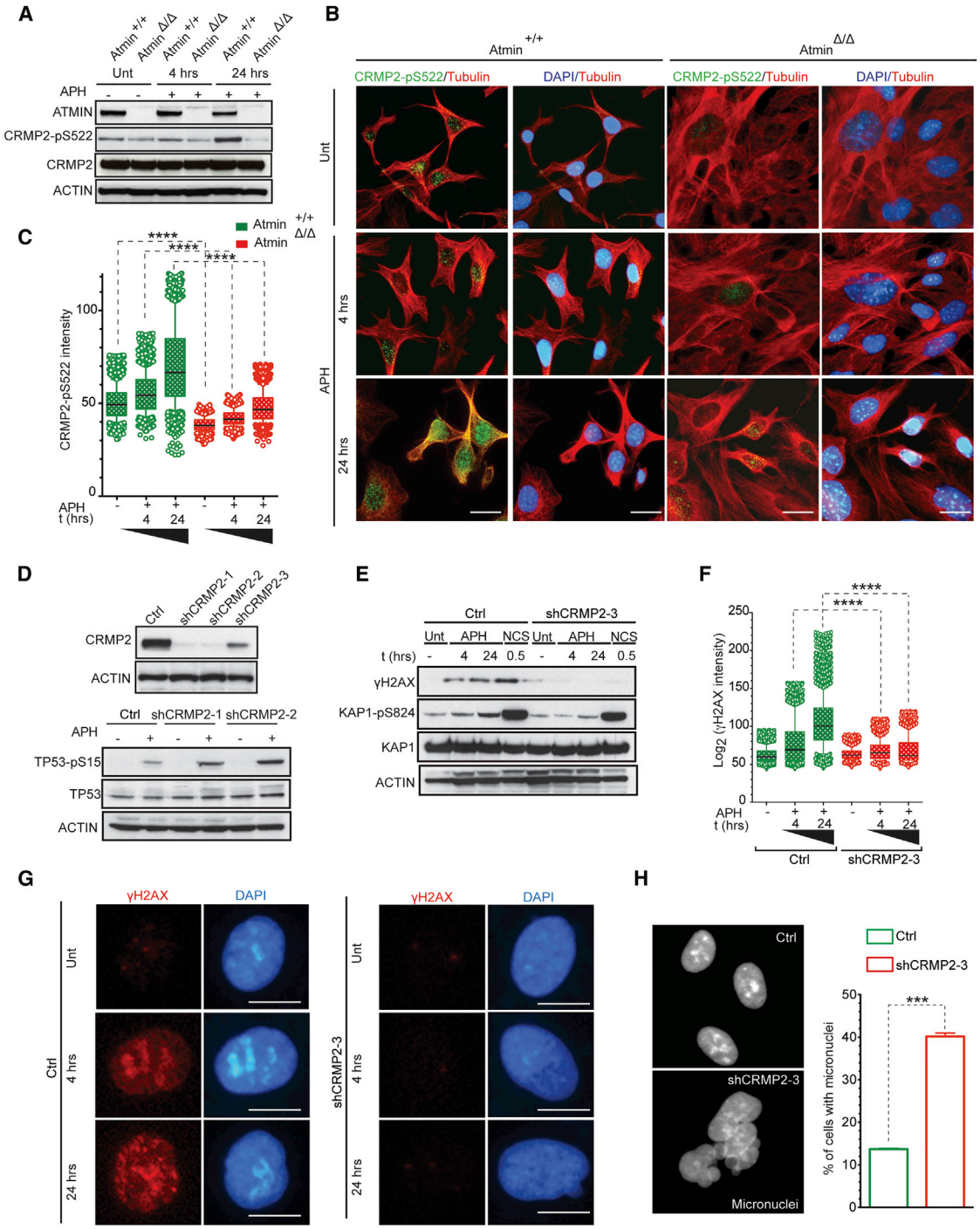

Figure 6. CRMP2 Is a Replication- and ATMIN-Dependent Phosphoprotein

(A) *Atmin*$^{+/+}$ and *Atmin*$^{\Delta/\Delta}$ MEFs were treated with 1 μM APH for the indicated times, and whole-cell extracts were analyzed for CRMP2 phosphorylation at Ser-522, by immunoblotting.

(B) MEFs were treated as in (A) and then immunostained for CRMP2-pS522 and Tubulin. DNA was counterstained with DAPI. Scale bar, 10 μm.

(C) Quantification of CRMP2-pS522 intensities per nucleus for more than 1,000 cells as in (B). Black lines inside columns represents median intensities. ****$p < 0.0001$ (p value was calculated by the Mann-Whitney U test).

(D) Top: depletion of CRMP2 in A549 cells, mediated by three independent shRNAs, is confirmed by immunoblotting using an anti-CRMP2 antibody. Bottom: CRMP2-depleted A549 cells (expressing shCRMP2-1 and shCRMP2-2 as well as a Control sequence; Ctrl) were treated with 1 μM APH for 24 hr and analyzed by immunoblotting for phosphorylated TP53 (at S15).

(legend continued on next page)

Please cite this article in press as: Mazouzi et al., A Comprehensive Analysis of the Dynamic Response to Aphidicolin-Mediated Replication Stress Uncovers Targets for ATM and ATMIN, Cell Reports (2016), http://dx.doi.org/10.1016/j.celrep.2016.03.077

DISCUSSION

The approach we have taken to systematically map the cellular response to replication stress, for maintaining genomic integrity, relies on the combination of transcriptomics and phosphoproteomics. Here we present a global time course of the cellular response to APH-induced replication stress. Moreover, we show that the kinase ATM and its cofactor ATMIN regulate many of these changes in response to replication stress induced by APH. Although several proteome-wide studies have identified phosphorylation events regulated by DNA double-strand breaks (Beli et al., 2012; Bensimon et al., 2010; Choi et al., 2012; Matsuoka et al., 2007), to our knowledge none have investigated the cellular response to replication stress. Here, we used high-throughput MS-based proteomics and RNA sequencing to map early and late changes in the phosphoproteome and the transcriptome induced by replication stress. Furthermore, we have revealed the dynamics of the ATM-ATMIN signaling pathway in this process. The unbiased, systems-level approach presented here shows that ATMIN and ATM are required for the phosphorylation of many shared sites, establishing the importance of ATMIN as a cofactor supporting ATM kinase activity in response to replication stress (see Figure 7E). We also reveal an underappreciated role for ATM in the early response to replication stress.

ATMIN physically interacts with ATM using a short carboxy-terminal motif, in a manner analogous to how NBS1 associates with ATM (Kanu and Behrens, 2007; Zhang et al., 2012). Our data provide evidence that ATMIN modulates the phosphorylation of many sites independently of ATM. Interestingly, the putative kinase-substrate network derived from our data suggests a substantial involvement of multiple other kinases in the cellular response to replication stress. Furthermore, our data propose that ATMIN could function as a cofactor for several kinases in regulating the phosphorylation events induced by replication stress. The data derived by analyzing the requirement for ATMIN in transcription exclude the possibility that ATMIN regulates the levels of protein phosphorylation indirectly through altering gene expression. This is an important distinction since, in addition to its role as an ATM cofactor, ATMIN has been reported to also function as a transcription factor (Jurado et al., 2012). Although ATM is known to respond to a wide range of cellular stresses, most studies have focused on its role following the induction of DNA double-strand breaks. Here we highlight the importance of ATM in the context of signaling after replication stress and in regulating phosphorylation of multiple substrates, both at early and late time points. Indeed, a large-scale analysis of proteins specifically localized at stalled forks after replication stress revealed ATM recruitment to nascent chromatin at early stages of DNA replication (Alabert et al., 2014).

Our proteome-wide approach of identifying replication-stress-induced phosphorylation sites, mediated via the use of APH, revealed a requirement for ATMIN in the regulation of H2AX phosphorylation, a posttranslational modification that occurs on chromatin to amplify the DNA damage signal. Notably, in the absence of γH2AX, many DNA damage response proteins, including the mediator proteins MDC1 and 53BP1, fail to localize effectively at DNA damage sites (Celeste et al., 2002, 2003; Paull et al., 2000). It has been shown that ATMIN is required for 53BP1 localization following replication stress (Kanu et al., 2015; Schmidt et al., 2014). This suggests that ATMIN might modulate the phosphorylation of H2AX, which consequently affects the downstream localization of 53BP1 to sites of damage hence promoting errors during replication, resulting in increased micronulei and anaphase bridges (Schmidt et al., 2014).

In this study, we also identify CRMP2 as a replication-stress-dependent phosphoprotein that requires ATMIN for its phosphorylation at S522. CRMP2 is part of the aminohydrolase family of enzymes, a large metal-dependent hydrolase superfamily, yet CRMP2 lacks hydrolase activity. CRMP2 has been shown to bind microtubules and is necessary for signaling by class 3 semaphorins and subsequent remodeling of the cytoskeleton. It is known that CRMP2 interacts with the mitotic spindle and that this association is affected by its phosphorylation. The kinase CDK5 phosphorylates CRMP2 at S522. This primes CRMP2 for subsequent phosphorylation by the kinase GSK3β at residues T509 and T514 during pro-metaphase (Oliemuller et al., 2013). We observed phosphorylation of the priming residue of CRMP2 at 24 hr post APH-induced replication stress. Under such treatment conditions, cells are blocked in S phase, suggesting that CRMP2 phosphorylation at S522 has an additional role besides its function during mitosis. Since mutation of this site renders cells sensitive to replication-stress-induced DNA damage, we propose that CRMP2 plays a role in the DNA damage response. These data also suggest that ATMIN may regulate CDK5 in response to replication stress, thereby promoting the phosphorylation of CRMP2 at S522.

CRMP2 is specifically hyperphosphorylated (at S522) in the brains of AD patients within peptide-rich plaques and neurofibrillary tangles (NFTs) (Hensley et al., 2011). Our finding that ATMIN regulates CRMP2 phosphorylation suggests a link between ATMIN function and the neuropathology of AD. Furthermore, since we find that CRMP2 is phosphorylated in response to APH-induced replication stress, this suggests that the hyperphosphorylation observed in AD might be the result of replication stress originating from the abortive cell cycle in neuronal cells (known as cell-cycle re-entry) (Yang et al., 2001).

In summary, we have charted the cellular response to replication stress (induced by APH), and we highlight the importance of

(E) CRMP2-depleted A549 (shCRMP2-3) and control A549 cells (Ctrl) were treated with 1 μM APH for the indicated times or NCS (a radiomimetic compound used as a positive control, at 50 ng/mL) for 30 min and analyzed by immunoblotting with indicated antibodies.
(F) γH2AX intensities (a.u.) per nucleus of (G). Results are displayed as box and whisker plots. The black lines within each column represent median intensities. More than 1,000 cells were counted for each condition. ****$p < 0.0001$ (p value was calculated by the Mann-Whitney U test).
(G) A549 cells depleted for CRMP2 (by expressing shCRMP2-3 or the control; Ctrl) were treated with 1 μM APH for the indicated times and analyzed by immunostaining for γH2AX. DNA was counterstained with DAPI. Scale bar, 10 μm.
(H) A549 cells depleted for CRMP2 (expressing shCRMP2-3 or Ctrl) were treated with 1 μM APH for 24 hr followed by incubation in compound-free media for 8 hr and stained with DAPI. Defects in cell division, marked by micronuclei formation, were imaged and quantified. At least 200 cells were analyzed per condition. Results from two independent experiments (mean ± SEM, t test ***$p < 0.001$) are shown.

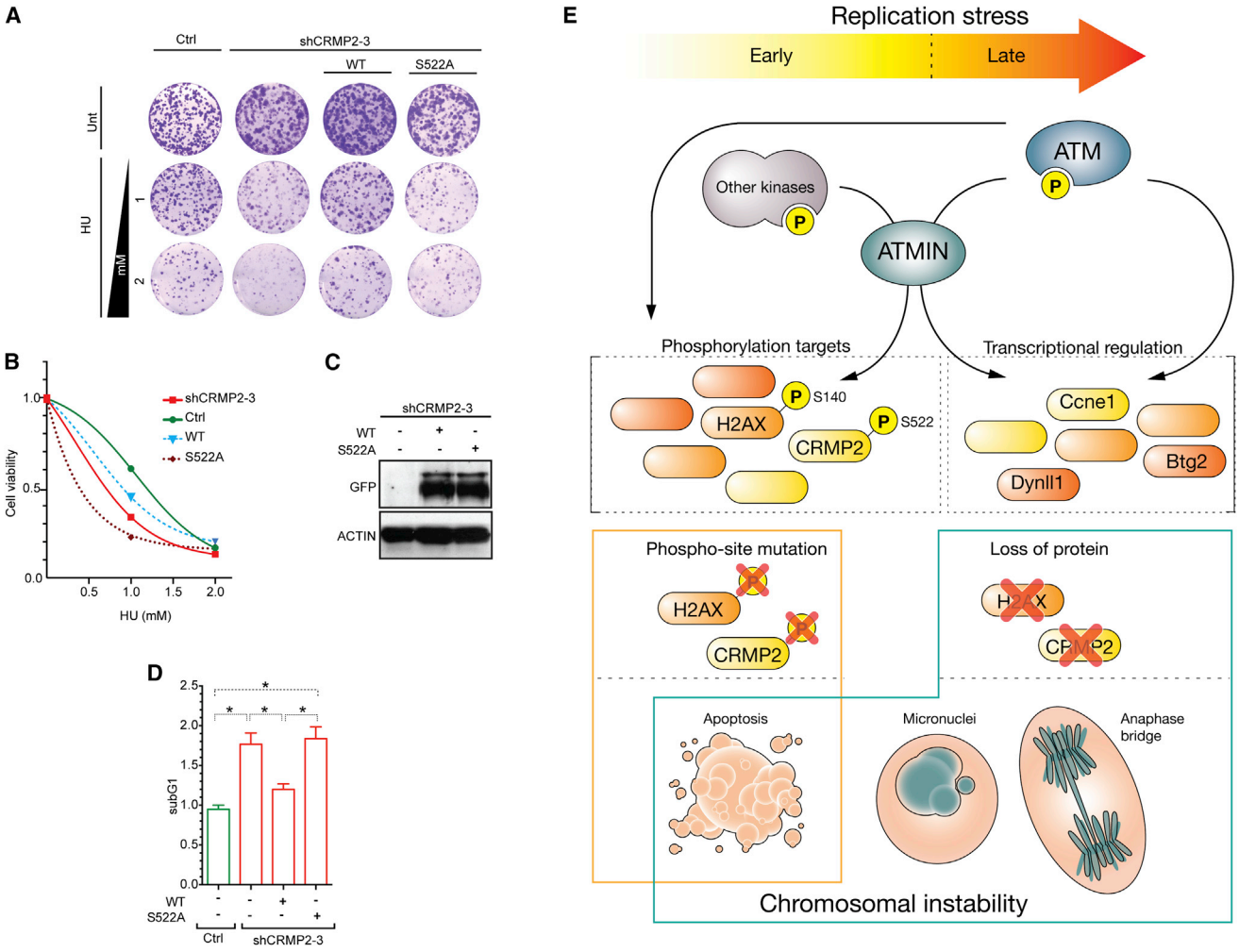

Figure 7. CRMP2 Phosphorylation at S522 Is Required for Cellular Responses to Replication Stress

(A) Clonogenic survival of A549 CRMP2-depleted cells (expressing shCRMP2-3, that targets the 3′UTR region of CRMP2) or control cells (Ctrl) were transfected with either wild-type CRMP2 (WT) or CRMP2 carrying a serine to alanine mutation at position 522 (S522A). Cells were treated with hyrdroxyurea to induce cell death via replication stress (HU; 1 mM, 2 mM) or left untreated for 24 hr, then the cells were incubated in compound-free media for 10 days.

(B) Macroscopic colonies were stained with crystal violet and quantified.

(C) The expression of the transfected constructs was confirmed by immunoblotting.

(D) Ctrl and CRMP2-depleted A549 cells (shCRMP2-3) were transfected with CRMP2 WT or S522A constructs. Cells were then treated with 1 μM APH for 24 hr, followed by incubation in compound-free media for 8 hr. Apoptotic subG1 populations were analyzed by propidium iodide staining. Results from two independent experiments (mean ± SEM, t test $^*p < 0.05$) are shown.

(E) Model illustrating the role of ATMIN and ATM in regulating phosphorylation and transcriptional events during replication stress (see main text for details).

ATM and ATMIN in regulating widespread phosphorylation events on multiple substrates, including DNA damage response factors, in a time-dependent manner. Through validating specific phosphorylation events, we identified previously unappreciated functions for ATMIN in modulating the phosphorylation of H2AX and CRMP2 (at S140 and S522, respectively). Moreover, we demonstrate that replication-stress-induced phosphorylation of CRMP2 at S522 is required for cell survival and chromosomal stability. Our findings suggest that many kinases in addition to ATM regulate the response to replication stress, perhaps employing ATMIN as a cofactor. The resource provided by our work will facilitate the discovery of new signaling pathways that function in the distinct response to DNA damage resulting from replication stress. Further, it will provide insight into pathologies that arise from replication stress.

EXPERIMENTAL PROCEDURES

Cell Culture, Plasmids, and Reagents

Atmin$^{+/+}$ and *Atmin*$^{\Delta/\Delta}$ MEFs (Kanu and Behrens, 2007) as well as *Atm*$^{+/+}$ and *Atm*$^{-/-}$ MEFs (Callén et al., 2009) were cultured in DMEM (Gibco), and A549 cells were cultured in RPMI-1640 (Gibco). All cells were grown in the presence of 10% fetal bovine serum (FBS) (Thermo Fisher Scientific) and 1% penicillin-streptomycin (Sigma-Aldrich) at 37°C with 5% CO_2 and 3% O_2. APH, NCS, and HU were purchased from Sigma. WT CRMP2 or CRMP2 S522A was

Please cite this article in press as: Mazouzi et al., A Comprehensive Analysis of the Dynamic Response to Aphidicolin-Mediated Replication Stress Uncovers Targets for ATM and ATMIN, Cell Reports (2016), http://dx.doi.org/10.1016/j.celrep.2016.03.077

expressed from the pEGFP-C1 vector (Clontech Laboratories) and provided by Dr. Ana Rouzaut (Center for Applied Medical Research, University of Navarra, Pamplona, Spain) and Dr. Manuel Serrano (Spanish National Cancer Research Centre, Madrid, Spain). For shRNA mediated depletion of CRMP2, two shRNAs (shCRMP2-1 and shCRMP2-2) targeting the coding region of the gene (5′-CTGAGTGTGATCCGGGATATT-3′, 5′-AGCCAAAGTCTT CAACCTTTA-3′) and one shRNA (shCRMP2-3) targeting the 3′UTR region (5′-TTAAGAGCCTGTGATAGTTAC-3′) were used. The shRNA sequences were obtained from the TRCN database (http://www.broadinstitute.org/rnai/public/gene/search) and cloned into the lentiviral vector pLKO.1 (Addgene) using AgeI and EcoRI restriction sites. Insertion of shRNA sequences was verified by sequencing. Lentiviral particles were produced by calcium phosphate transfection of the shRNA containing pLKO.1 constructs along with packaging plasmids into HEK293T cells. Two days after transfection, virus-containing supernatant was harvested and filtered to remove HEK293T cells from the supernatant. A549 cells were infected with the virus-containing supernatant in the presence of polybrene (final concentration 8 μg/mL). Infected cells were selected using puromycin (2 μg/mL; Sigma-Aldrich) for 48 hr. For transfection of the CRMP2 expression constructs, the Effectene transfection reagent from QIAGEN was used.

Protein Extracts and Immunoblotting

Cells were lysed in RIPA lysis buffer supplemented with protease inhibitors (Sigma) and phosphatase inhibitors (Sigma-Aldrich, NEB). Lysates were sonicated, centrifuged, and heated with reducing sample buffer. Protein samples were separated by SDS–PAGE (3%–8% or 4%–12% gradient gels; Invitrogen) and subsequently transferred onto nitro-cellulose membranes. All primary antibodies were used at 1:1,000 dilution and secondary antibodies at 1:5,000. Antibodies used were as follows: ATM 2C1 (Santa Cruz), P-S1981-ATM (10H11.E12; NEB), ASCIZ (Millipore), P-S824-KAP1 (Bethyl Laboratories), KAP1 (Bethyl Laboratories), P-S15-TP53 (16G8; NEB), TP53 (Pab-421; CR-UK generated antibody), P-S957-SMC1 (5D11G5; Millipore), P-S345-CHEK1 (2341S; Cell Signaling Technology), CHEK1 (DCS-310; Santa Cruz), CRMP2 (ab129082; Abcam), P-S522-CRMP2 (CP2191; Biotrend), H2AX (7631P; Cell Signaling Technology), P-S140-H2AX (07-164; Millipore), GFP (3E1; CR-UK generated antibody), and β-actin (Sigma).

Immunofluorescence and Associated Microscopy

Cells were seeded onto coverslips (VWR) in 24-well plates or directly in 96-well plates. On the following day, cells were treated as indicated, washed twice with ice-cold PBS, fixed with ice-cold methanol for 20 min at −20°C, and then permeabilized with 0.5% Triton X-100 in PBS for 20 min at room temperature and blocked with 10% FCS/0.1% Triton X-100 in PBS for 1 hr with three washes (PBS) between individual steps. Primary (53BP1 [H300; Santa Cruz], P-S140-H2AX [05-636-I; Millipore], P-S522-CRMP2 [CP2191; Biotrend]) and secondary (Alexa Fluor 546 goat anti-rabbit and Alexa Fluor 488 goat anti-mouse; Invitrogen) antibodies were diluted in blocking solution (1:600) and incubated on cells for 1 hr at room temperature. Finally, cells were stained with DAPI (Sigma-Aldrich) for 20 min at room temperature in the dark. Cell images were taken on a deconvolution microscope (Leica) for slides or Operetta High Content Imaging microscope (PerkinElmer) for the 96-well plates.

Colony Formation Assay

A549 cells (at a density of 1,000 cells/well) were seeded into 6-well plates and treated as indicated for approximately 2 weeks until clear colonies formed. Then, the medium was removed and cells were washed with PBS and fixed using 3.7% PFA (paraformaldehyde). After the removal of PFA, a solution of 0.1% crystal violet in 5% ethanol was added and cells were stained overnight. The next day, staining solution was removed, wells were washed extensively, and images were taken. For quantification, Crystal Violet was extracted from cells with pure ethanol and absorbance was measured using a spectrophotometer at 595 nm.

qRT-PCR

Cells were harvested and RNA was isolated using phenol-chlorophorm extraction. RNA was treated with 1 μl DNase (Sigma) and then reverse transcribed with the SuperScript III Reverse Transcriptase protocol (Invitrogen) to obtain cDNA. An amount of 1 μg of cDNA template was used for the qRT-PCR using SYBR Green qPCR Mastermix (QIAGEN). Analysis was performed out in duplicates using expression of mEF1α for normalization of data. The PCR was performed on a 7900HT Fast Real-Time PCR System (Applied Biosystems). The following primers were used:

Ccne1: 5′-GTTCCGTTCGCCATGGTTAT-3′; 5′-CCCGGAAGTGCTTGAG CTT-3′,
Btg2: 5′-CGGTGGCTGCCTCCTATG-3′; 5′-TCCTGCCCAGCATCATC TG-3′,
mEF1α: 5′-GCAAAAACGACCCACCAATG-3′ 5′- GGCCTGGATGGTTCAG GATA-3′.

Comet Assays

The neutral comet assay was performed as described (El-Khamisy et al., 2005). For the alkali comet assay, cells at a density of 3×10^4 were treated with 1 μM APH for 4 or 24 hr or with 100 μM H_2O_2 for 10 min, as a positive control. Cells were washed in pre-chilled PBS and then mixed in 100 μl 1.2% low melting agarose (Sigma-Aldrich, type VII) maintained at 42°C. The cell suspension was then immediately layered onto pre-chilled frosted glass slides pre-coated with 0.6% agarose and maintained in the dark at 4°C for all following steps. Slides were immersed in pre-chilled lysis buffer (2.5 M NaCl, 10 mM Tris-HCl, 100 mM EDTA [pH 8.0], 1% Triton X-100, 1% DMSO [pH 10]; DMSO and Triton X added shortly before use) overnight. Slides were washed with pre-chilled distilled water (2 × 10 min) and next placed for 45 min in pre-chilled alkaline electrophoresis buffer (55 mM NaOH, 1 mM EDTA, 1% DMSO). Electrophoresis was conducted at 30 V for 25 min, followed by neutralization in 400 mM Tris-HCl [pH 7.0] for 1 hr. Finally, DNA was stained with SYBR Gold (1:10,000 dilution in H_2O; Life Technologies) for 10 min. The comet tail moment was measured for at least 100 cells per sample using the CASP image-analysis program (Końca et al., 2003).

Cell Cycle Analysis

Cells were treated with either DMSO or 1 μM APH at different time points as indicated, or treated with 1 μM APH for 24 hr and then released for different time points. Cell-cycle stages were analyzed using propidium iodide staining. Briefly, cells were harvested, resuspended in PBS, and fixed overnight with cold 70% ethanol. After centrifugation, ethanol was removed and cells were resuspended in PBS containing 1 μg/mL RNase A and 1 μg/mL propidium iodide. Finally, cells were analyzed on a FACScalibur flow cytometer. Following cell acquisition, analysis was performed using FlowJo software (Tree Star).

Statistical Analysis

Data are expressed as ± SEM unless otherwise stated. Statistical analysis of the RNA sequencing and the phosphoproteomics data can be found in the Supplemental Experimental Procedures section. All reported p values are two-tailed unless stated otherwise.

Other Methods

See the Supplemental Experimental Procedures.

ACCESSION NUMBERS

The accession number for the RNA-seq data reported in this paper is GEO: GSE72275. Processed data are available in Table S1.

SUPPLEMENTAL INFORMATION

Supplemental Information includes Supplemental Experimental Procedures, seven figures, and four tables and can be found with this article online at http://dx.doi.org/10.1016/j.celrep.2016.03.077.

AUTHOR CONTRIBUTIONS

Conceptualization, A.M. and J.I.L.; Methodology, A.M., A.S., A.C.M., D.C., M.W., J.P., and S.-C.C.; Data Curation, A.M., A.S., D.C., M.S., and F.P.B.;

Writing, A.M. and J.I.L.; Visualization, A.M., A.S., D.C., and J.I.L.; Supervision, A.P., S.F.E.-K., C.B., R.K., J.C., K.L.B., and J.I.L.; Project Administration, J.L.; Funding Acquisition, A.M., S.F.E.-K., and J.I.L.

ACKNOWLEDGMENTS

We thank Dr. A. Nussenzweig (Centre for Cancer Research, NIH) for providing the *Atm* control and knockout MEFs. CRMP2 constructs (pEGFP-C1-CRMP2 and pEGFP-C1-CRMP2-S522A) were kindly provided by Dr. Ana Rouzaut (Center for Applied Medical Research, University of Navarra) and Dr. Manuel Serrano (Spanish National Cancer Centre). We thank the Biomedical Sequencing Facility at CeMM for technical advice and for performing the next generation sequencing experiments. We also thank Drs S.P. Jackson, G. Superti-Furga, J. Lukas, K. Caldecott, and C. Schliehe for critical reading of the manuscript. Dr. B. Vilagos helped in preparing the graphical model. A.M. and J.P. were supported by a project grant from the FWF (project number P 24766-B20) to J.I.L. Additionally, A.M. was funded by a DOC fellowship from the Austrian Academy of Sciences (24102). The J.I.L. lab is supported by a Marie-Curie Career Integration Grant (project no. 321602-NonCanATM). S.-C.C. is funded by a Wellcome Trust investigator award (103844) to S.F.E.-K. CeMM is funded by the Austrian Academy of Sciences.

Received: August 24, 2015
Revised: January 21, 2016
Accepted: March 21, 2016
Published: April 14, 2016

REFERENCES

Alabert, C., Bukowski-Wills, J.C., Lee, S.B., Kustatscher, G., Nakamura, K., de Lima Alves, F., Menard, P., Mejlvang, J., Rappsilber, J., and Groth, A. (2014). Nascent chromatin capture proteomics determines chromatin dynamics during DNA replication and identifies unknown fork components. Nat. Cell Biol. *16*, 281–293.

Bartek, J., Mistrik, M., and Bartkova, J. (2012). Thresholds of replication stress signaling in cancer development and treatment. Nat. Struct. Mol. Biol. *19*, 5–7.

Beli, P., Lukashchuk, N., Wagner, S.A., Weinert, B.T., Olsen, J.V., Baskcomb, L., Mann, M., Jackson, S.P., and Choudhary, C. (2012). Proteomic investigations reveal a role for RNA processing factor THRAP3 in the DNA damage response. Mol. Cell *46*, 212–225.

Bensimon, A., Schmidt, A., Ziv, Y., Elkon, R., Wang, S.Y., Chen, D.J., Aebersold, R., and Shiloh, Y. (2010). ATM-dependent and -independent dynamics of the nuclear phosphoproteome after DNA damage. Sci. Signal. *3*, rs3.

Bodenmiller, B., Mueller, L.N., Mueller, M., Domon, B., and Aebersold, R. (2007). Reproducible isolation of distinct, overlapping segments of the phosphoproteome. Nat. Methods *4*, 231–237.

Burhans, W.C., and Weinberger, M. (2007). DNA replication stress, genome instability and aging. Nucleic Acids Res. *35*, 7545–7556.

Callén, E., Jankovic, M., Wong, N., Zha, S., Chen, H.T., Difilippantonio, S., Di Virgilio, M., Heidkamp, G., Alt, F.W., Nussenzweig, A., and Nussenzweig, M. (2009). Essential role for DNA-PKcs in DNA double-strand break repair and apoptosis in ATM-deficient lymphocytes. Mol. Cell *34*, 285–297.

Celeste, A., Petersen, S., Romanienko, P.J., Fernandez-Capetillo, O., Chen, H.T., Sedelnikova, O.A., Reina-San-Martin, B., Coppola, V., Meffre, E., Difilippantonio, M.J., et al. (2002). Genomic instability in mice lacking histone H2AX. Science *296*, 922–927.

Celeste, A., Fernandez-Capetillo, O., Kruhlak, M.J., Pilch, D.R., Staudt, D.W., Lee, A., Bonner, R.F., Bonner, W.M., and Nussenzweig, A. (2003). Histone H2AX phosphorylation is dispensable for the initial recognition of DNA breaks. Nat. Cell Biol. *5*, 675–679.

Choi, S., Srivas, R., Fu, K.Y., Hood, B.L., Dost, B., Gibson, G.A., Watkins, S.C., Van Houten, B., Bandeira, N., Conrads, T.P., et al. (2012). Quantitative proteomics reveal ATM kinase-dependent exchange in DNA damage response complexes. J. Proteome Res. *11*, 4983–4991.

Corrente, G., Guardavaccaro, D., and Tirone, F. (2002). PC3 potentiates NGF-induced differentiation and protects neurons from apoptosis. Neuroreport *13*, 417–422.

Derheimer, F.A., and Kastan, M.B. (2010). Multiple roles of ATM in monitoring and maintaining DNA integrity. FEBS Lett. *584*, 3675–3681.

Difilippantonio, S., Celeste, A., Fernandez-Capetillo, O., Chen, H.T., Reina San Martin, B., Van Laethem, F., Yang, Y.P., Petukhova, G.V., Eckhaus, M., Feigenbaum, L., et al. (2005). Role of Nbs1 in the activation of the Atm kinase revealed in humanized mouse models. Nat. Cell Biol. *7*, 675–685.

Durkin, S.G., and Glover, T.W. (2007). Chromosome fragile sites. Annu. Rev. Genet. *41*, 169–192.

El-Khamisy, S.F., Saifi, G.M., Weinfeld, M., Johansson, F., Helleday, T., Lupski, J.R., and Caldecott, K.W. (2005). Defective DNA single-strand break repair in spinocerebellar ataxia with axonal neuropathy-1. Nature *434*, 108–113.

Falck, J., Coates, J., and Jackson, S.P. (2005). Conserved modes of recruitment of ATM, ATR and DNA-PKcs to sites of DNA damage. Nature *434*, 605–611.

Fernandez-Capetillo, O., and Nussenzweig, A. (2013). Naked replication forks break apRPArt. Cell *155*, 979–980.

Flach, J., Bakker, S.T., Mohrin, M., Conroy, P.C., Pietras, E.M., Reynaud, D., Alvarez, S., Diolaiti, M.E., Ugarte, F., Forsberg, E.C., et al. (2014). Replication stress is a potent driver of functional decline in ageing haematopoietic stem cells. Nature *512*, 198–202.

Friedel, A.M., Pike, B.L., and Gasser, S.M. (2009). ATR/Mec1: coordinating fork stability and repair. Curr. Opin. Cell Biol. *21*, 237–244.

Fukata, Y., Itoh, T.J., Kimura, T., Ménager, C., Nishimura, T., Shiromizu, T., Watanabe, H., Inagaki, N., Iwamatsu, A., Hotani, H., and Kaibuchi, K. (2002). CRMP-2 binds to tubulin heterodimers to promote microtubule assembly. Nat. Cell Biol. *4*, 583–591.

Glover, T.W., Berger, C., Coyle, J., and Echo, B. (1984). DNA polymerase alpha inhibition by aphidicolin induces gaps and breaks at common fragile sites in human chromosomes. Hum. Genet. *67*, 136–142.

Guo, Z., Kozlov, S., Lavin, M.F., Person, M.D., and Paull, T.T. (2010). ATM activation by oxidative stress. Science *330*, 517–521.

Halazonetis, T.D., Gorgoulis, V.G., and Bartek, J. (2008). An oncogene-induced DNA damage model for cancer development. Science *319*, 1352–1355.

Harrigan, J.A., Belotserkovskaya, R., Coates, J., Dimitrova, D.S., Polo, S.E., Bradshaw, C.R., Fraser, P., and Jackson, S.P. (2011). Replication stress induces 53BP1-containing OPT domains in G1 cells. J. Cell Biol. *193*, 97–108.

Hensley, K., Venkova, K., Christov, A., Gunning, W., and Park, J. (2011). Collapsin response mediator protein-2: an emerging pathologic feature and therapeutic target for neurodisease indications. Mol. Neurobiol. *43*, 180–191.

Horn, H., Schoof, E.M., Kim, J., Robin, X., Miller, M.L., Diella, F., Palma, A., Cesareni, G., Jensen, L.J., and Linding, R. (2014). KinomeXplorer: an integrated platform for kinome biology studies. Nat. Methods *11*, 603–604.

Jurado, S., Gleeson, K., O'Donnell, K., Izon, D.J., Walkley, C.R., Strasser, A., Tarlinton, D.M., and Heierhorst, J. (2012). The Zinc-finger protein ASCIZ regulates B cell development via DYNLL1 and Bim. J. Exp. Med. *209*, 1629–1639.

Kaidi, A., and Jackson, S.P. (2013). KAT5 tyrosine phosphorylation couples chromatin sensing to ATM signalling. Nature *498*, 70–74.

Kanu, N., and Behrens, A. (2007). ATMIN defines an NBS1-independent pathway of ATM signalling. EMBO J. *26*, 2933–2941.

Kanu, N., and Behrens, A. (2008). ATMINistrating ATM signalling: regulation of ATM by ATMIN. Cell Cycle *7*, 3483–3486.

Kanu, N., Zhang, T., Burrell, R.A., Chakraborty, A., Cronshaw, J., Costa, C.D., Grönroos, E., Pemberton, H.N., Anderton, E., Gonzalez, L., et al. (2015). RAD18, WRNIP1 and ATMIN promote ATM signalling in response to replication stress. Oncogene, Published online November 9, 2015.

Końca, K., Lankoff, A., Banasik, A., Lisowska, H., Kuszewski, T., Góźdź, S., Koza, Z., and Wojcik, A. (2003). A cross-platform public domain PC image-analysis program for the comet assay. Mutat. Res. *534*, 15–20.

Please cite this article in press as: Mazouzi et al., A Comprehensive Analysis of the Dynamic Response to Aphidicolin-Mediated Replication Stress Uncovers Targets for ATM and ATMIN, Cell Reports (2016), http://dx.doi.org/10.1016/j.celrep.2016.03.077

Kruse, J.P., and Gu, W. (2009). Modes of p53 regulation. Cell *137*, 609–622.

Lavin, M.F., and Kozlov, S. (2007). ATM activation and DNA damage response. Cell Cycle *6*, 931–942.

Lee, J.H., and Paull, T.T. (2007). Activation and regulation of ATM kinase activity in response to DNA double-strand breaks. Oncogene *26*, 7741–7748.

Loizou, J.I., Sancho, R., Kanu, N., Bolland, D.J., Yang, F., Rada, C., Corcoran, A.E., and Behrens, A. (2011). ATMIN is required for maintenance of genomic stability and suppression of B cell lymphoma. Cancer Cell *19*, 587–600.

López-Contreras, A.J., and Fernandez-Capetillo, O. (2010). The ATR barrier to replication-born DNA damage. DNA Repair (Amst.) *9*, 1249–1255.

Lukas, C., Savic, V., Bekker-Jensen, S., Doil, C., Neumann, B., Pedersen, R.S., Grøfte, M., Chan, K.L., Hickson, I.D., Bartek, J., and Lukas, J. (2011). 53BP1 nuclear bodies form around DNA lesions generated by mitotic transmission of chromosomes under replication stress. Nat. Cell Biol. *13*, 243–253.

Matsuoka, S., Ballif, B.A., Smogorzewska, A., McDonald, E.R., 3rd, Hurov, K.E., Luo, J., Bakalarski, C.E., Zhao, Z., Solimini, N., Lerenthal, Y., et al. (2007). ATM and ATR substrate analysis reveals extensive protein networks responsive to DNA damage. Science *316*, 1160–1166.

Mazouzi, A., Velimezi, G., and Loizou, J.I. (2014). DNA replication stress: causes, resolution and disease. Exp. Cell Res. *329*, 85–93.

Oliemuller, E., Peláez, R., Garasa, S., Pajares, M.J., Agorreta, J., Pío, R., Montuenga, L.M., Teijeira, A., Llanos, S., and Rouzaut, A. (2013). Phosphorylated tubulin adaptor protein CRMP-2 as prognostic marker and candidate therapeutic target for NSCLC. Int. J. Cancer *132*, 1986–1995.

Olsen, J.V., Blagoev, B., Gnad, F., Macek, B., Kumar, C., Mortensen, P., and Mann, M. (2006). Global, in vivo, and site-specific phosphorylation dynamics in signaling networks. Cell *127*, 635–648.

Paull, T.T., Rogakou, E.P., Yamazaki, V., Kirchgessner, C.U., Gellert, M., and Bonner, W.M. (2000). A critical role for histone H2AX in recruitment of repair factors to nuclear foci after DNA damage. Curr. Biol. *10*, 886–895.

Petermann, E., and Helleday, T. (2010). Pathways of mammalian replication fork restart. Nat. Rev. Mol. Cell Biol. *11*, 683–687.

Schmidt, L., Wiedner, M., Velimezi, G., Prochazkova, J., Owusu, M., Bauer, S., and Loizou, J.I. (2014). ATMIN is required for the ATM-mediated signaling and recruitment of 53BP1 to DNA damage sites upon replication stress. DNA Repair (Amst.) *24*, 122–130.

Shaw, P.H. (1996). The role of p53 in cell cycle regulation. Pathol. Res. Pract. *192*, 669–675.

Toledo, L.I., Altmeyer, M., Rask, M.B., Lukas, C., Larsen, D.H., Povlsen, L.K., Bekker-Jensen, S., Mailand, N., Bartek, J., and Lukas, J. (2013). ATR prohibits replication catastrophe by preventing global exhaustion of RPA. Cell *155*, 1088–1103.

Uziel, T., Lerenthal, Y., Moyal, L., Andegeko, Y., Mittelman, L., and Shiloh, Y. (2003). Requirement of the MRN complex for ATM activation by DNA damage. EMBO J. *22*, 5612–5621.

Wang, L., Paradee, W., Mullins, C., Shridhar, R., Rosati, R., Wilke, C.M., Glover, T.W., and Smith, D.I. (1997). Aphidicolin-induced FRA3B breakpoints cluster in two distinct regions. Genomics *41*, 485–488.

Ward, I.M., Difilippantonio, S., Minn, K., Mueller, M.D., Molina, J.R., Yu, X., Frisk, C.S., Ried, T., Nussenzweig, A., and Chen, J. (2005). 53BP1 cooperates with p53 and functions as a haploinsufficient tumor suppressor in mice. Mol. Cell. Biol. *25*, 10079–10086.

Yang, Y., Geldmacher, D.S., and Herrup, K. (2001). DNA replication precedes neuronal cell death in Alzheimer's disease. J. Neurosci. *21*, 2661–2668.

Zeman, M.K., and Cimprich, K.A. (2014). Causes and consequences of replication stress. Nat. Cell Biol. *16*, 2–9.

Zhang, T., Penicud, K., Bruhn, C., Loizou, J.I., Kanu, N., Wang, Z.Q., and Behrens, A. (2012). Competition between NBS1 and ATMIN controls ATM signaling pathway choice. Cell Rep. *2*, 1498–1504.